Nanoscale

PAPER

Identification of Mott insulators and Anderson insulators in self-assembled gold nanoparticles thin films†

Cite this: *Nanoscale*, 2014, **6**, 5887

Cheng-Wei Jiang,[a] I-Chih Ni,[b] Shien-Der Tzeng,[b] Cen-Shawn Wu[c] and Watson Kuo*[a]

How the interparticle tunnelling affects the charge conduction of self-assembled gold nanoparticles is studied by three means: tuning the tunnel barrier width by different molecule modification and by substrate bending, and tuning the barrier height by high-dose electron beam exposure. All approaches indicate that the metal–Mott insulator transition is governed predominantly by the interparticle coupling strength, which can be quantified by the room temperature sheet resistance. The Hubbard gap, following the prediction of quantum fluctuation theory, reduces to zero rapidly as the sheet resistance decreases to the quantum resistance. At very low temperature, the fate of devices near the Mott transition depends on the strength of disorder. The charge conduction is from nearest-neighbour hopping to co-tunnelling between nanoparticles in Mott insulators whereas it is from variable-range hopping through charge puddles in Anderson insulators. When the two-dimensional nanoparticle network is under a unidirectional strain, the interparticle coupling becomes anisotropic so the average sheet resistance is required to describe the charge conduction.

Received 14th December 2013
Accepted 25th February 2014

DOI: 10.1039/c3nr06627d

www.rsc.org/nanoscale

1 Introduction

Recently the electrical characteristics of self-assembled nanoparticle (NP) films have attracted much attention for research into quantum transport because of their wide tunability of electrical characteristics, even though NPs are metallic.[1,2] For example, one can modify various molecules on NPs by chemical substitution, and assemble the modified NPs into monolayers or thin films easily. Previous works have confirmed that the following factors may strongly affect the electron transport in NP assemblies: particle size,[3] interparticle distance,[4] the conductance of linking molecules,[5] structure disorder,[6,7] and the distribution of trapped-charge.[8] The interparticle coupling strength, which decays exponentially with the barrier height and the length of the molecular junction, is the leading one among the above factors.[9–11] This coupling strength is quantified by the dimensionless tunnelling conductance $g = R_K/R_T$, in which R_T is the tunnelling resistance of the molecular junction and $R_K = h/e^2 \approx 25.8$ kΩ is the quantum resistance. In the strong-coupling regime of $g \gg 1$, the NP network has metallic properties,[12] but in the opposite case of $g \ll 1$, it becomes an insulator. In this weak-coupling regime, conduction electrons have to overcome single-electron charging energy owing to the small capacitance of a NP, and present thermally-activated behaviour.[13,14] Pictured by the Mott–Hubbard model,[15] this metal-to-insulator transition (MIT) occurs when the carbon number is 5 for an alkanethiol linkage molecule.[16] Other works have also found similar MITs by controlling other factors such as the NP surface coverage[5,7] or the NP diameter.[3]

On the other hand, disorder is common in NP films and results in versatile transport properties. Three types of disorder can be distinguished: structural disorder in the array topology, local disorder in the interparticle couplings, and local charge disorder due to random offset charges.[9] In granular systems, disorder and charge interaction affect the transport in subtle ways, and several new aspects of this interplay have been discussed recently.[17–19] For example, at a sufficiently low temperature, the charge conducts in the way of Efros and Shklovskii variable range hopping, which originates from a collective transport involving several NPs in the presence of disorder.[20,21] Such co-tunnelling describes the effective electron tunnelling from an initial to a final state *via* virtual intermediate states with a long-range tunnelling path depending on the overall energy cost.[8] The inelastic co-tunnelling usually shows non-linear current–voltage characteristics.[22] Anderson localization is another major effect that originates from disorder owing to the coherent back-scattering of non-interacting particles from randomly distributed impurities.[23] How to experimentally distinguish an Anderson insulator from Mott–Hubbard insulators in these NP systems is still lacking.

[a]*Department of Physics, National Chung Hsing University, Taichung 402, Taiwan. E-mail: wkuo@phys.nchu.edu.tw*

[b]*Department of Physics, National Dong Hwa University, Hualien 974, Taiwan*

[c]*Department of Physics, National Chang-Hua University of Education, ChangHua 500, Taiwan*

† Electronic supplementary information (ESI) available. See DOI: 10.1039/c3nr06627d

In this paper, we studied the electrical conduction mechanisms of gold nanoparticles (AuNPs) films by measuring the current–voltage characteristics, temperature-dependent resistances, and magnetoresistances. Except for controlling the length of the molecular junctions, we take advantage of the electron beam (e-beam) exposure to reduce the junction barrier height as well as applying strain to the substrate for *in situ* tuning the interparticle spacing. By these means, the sheet resistances of studied samples varied from 10^2 to 10^{11} Ω, and gave an interparticle coupling strength ranging from $g = 10^{-7}$ to 10^2. However, the thermal expansion of the substrate would bring in an extra contribution to the temperature dependence, and was commonly neglected until very recently.[24,25] With the removal of thermal expansion contributions, we obtain how the interparticle coupling strength affects the Hubbard gap of Mott insulators, from which the critical point of the Mott–Hubbard MIT is determined. Furthermore we can identify Anderson insulators, which have zero Hubbard gap but exhibit charge inhomogeneity due to quantum interference at low temperatures. As pointed out in many works, molecule-modified NPs have the potential as high-performance sensors for chemical and biological signals, medical diagnostics, and human health.[2] Such an analysis provides us with a better understanding of the conduction mechanism of NP assemblies and allows us better control in such a system for these applications.

2 Experimental

The AuNPs were synthesized by reduction of $HAuCl_4$ by tannic acid and were of 12 nm diameter in size.[26] We used 4 different molecules to modify the AuNP surface: from short to long, 3-mercaptopropionic acid (MPA), 6-mercaptohexadecanoic acid (MHA), 8-mercaptooctanoic acid (MOA), and 11-mercaptoundecanoic acid (MUA). The longer molecules would introduce a longer interparticle spacing when AuNPs are assembled into a two-dimensional film. AuNP colloidal solution (typically 5 mL with a concentration of $\sim 3 \times 10^{12}$ cm^{-3}) was added to a 30 mL centrifuge tube, together with the (3-aminopropyl)trimethoxysilane (APTMS)-modified substrate laid on a support in the tube. After being centrifuged at 8500 *g* for 20 min, AuNPs were fully deposited on the substrate, and we could obtain a multilayer AuNP film directly by gently pulling out the sample and drying it in the air. The thickness of the deposited AuNP film could be controlled by the total amount of AuNPs in the solution and the films were further observed by scanning electron microscopy. In this study, the typical thickness of the AuNP film is 2–3 NP layers. AuNP films were assembled on to SiO_2/Si substrates or flexible substrates (50 μm-thick polyimide, PI) with pre-made electrodes, which were 20 nm/50 nm Cr/Au electrodes fabricated by using e-beam- or photo-lithography and a lift-off technique.

The above molecule engineering did not provide a precise control of the interparticle spacing *s* due to inevitable disorder in the AuNP assemblies. An *in situ* control of *s* by bending the substrate was further applied to overcome this difficulty: strain on the substrate would create a change in *s*, $\Delta s = \varepsilon/(2r + s)$, in which ε is the strain and *r* is the radius of the AuNP. In our work the bending was introduced by attaching the flexible 50 μm-thick PI substrate to cylindrical surfaces with different curvature radii, giving a strain ranging from about −1.7% to 0.5%.

The tunnelling resistance does not only depend on the interparticle spacing but also depends on the tunnelling barrier height. Exposing the device to high-dosage e-beam bombardment may reduce the barrier height of the molecular junctions so as to greatly reduce R_T. R_T values for our samples were estimated from the monolayer sheet resistance, R_s, at room temperature (RT). It was found that the device RT resistance could be reduced at most to 5 orders of magnitude by dosage control.

The temperature-dependent resistance measurements were performed in a physical property measurement system (Quantum Design) from RT to 2 K, and in a dilution refrigerator (Oxford instruments) from 1 K down to 40 mK.

3 Results and discussions

3.1 Metallic and insulating behaviours

A great variation in room temperature resistance (R_{RT}) values for AuNP devices with different surface modifications was found. This strong impact of the molecule linkage on the charge conduction originates from the exponential increase of the tunnelling resistance R_T with the interparticle spacing *s*: $R_T \propto \exp(\beta s)$. As reported earlier, the tunnelling decay constant β obtained in our case is about 11.8 nm^{-1}, allowing a comparison with the value in the case of alkanedithiol.[26] On alkanedithiol single molecular junctions and on assembled AuNPs cross-linked with different alkanedithiol linkers HS–$(CH_2)_n$–SH, previous works have reported $R_T \propto \exp(\beta_n n)$ with $\beta_n \approx 1.0 \pm 0.1$.[16,27] Here *n* is the number of carbon atoms of the linker molecule, and β_n the tunnelling decay constant per carbon atom.

By controlling *s*, one can tune the electron tunnelling resistance, R_T between NPs so as to drive the system to undergo the metal–insulator transition. The MIT is best illustrated in the temperature-dependent resistances as shown in Fig. 1a. There are opposite temperature dependences according to the surface modification: metallic behaviour in which the resistance increased linearly with temperature was found for AuNP films modified by short (MPA) carbon-chain molecules; and insulating behaviour in which the resistance decreased non-linearly was found for the AuNP films modified by long (MUA, MOA and MHA) carbon-chain molecules. At low temperatures these insulating devices exhibit non-linear current–voltage (*IV*) characteristics. These behaviours signify an MIT by tuning the carbon number from $n = 3$ to $n = 6$ (*s* from 0.90 nm to 1.27 nm).[4,16]

Near the transition, the metallic and insulating behaviours require a closer inspection because other effects may have a significant impact. In particular, although most MPA devices (referred to as MPAm) exhibited metallic behaviour (linear *IV* and $dR/dT > 0$), we could find exceptions, such as MPAi and MPAii devices, showing insulating behaviour. Generally speaking, insulating MPA devices had larger RT resistances than metallic MPA devices. Since the AuNP assemblies using

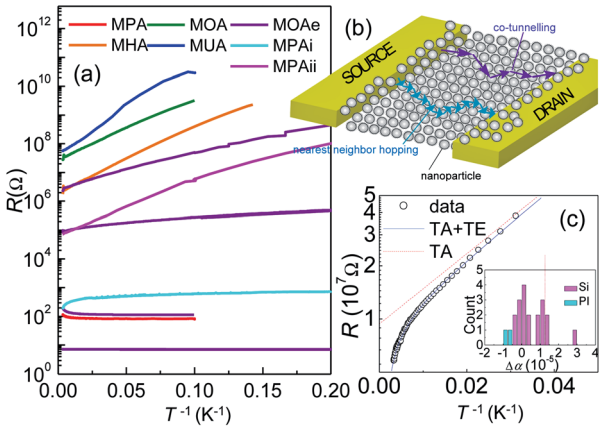

Fig. 1 (a) Plots R *vs.* $1/T$. When $R_{RT} > R_K$, the device is an insulator; when $R_{RT} < R_K$, it can be metallic (MPAm) or insulating (MPAi) possibly due to different strength of disorder. When $T > 20$ K, the insulating devices clearly obey an Arrhenius thermal activation behaviour. (b) The schematic shows the charge conduction through a two-dimensional matrix formed by self-assembled NPs. For Mott insulators, there are nearest-neighbour hopping and variable range co-tunnelling. (c) The fitting result of an MUA device at $T > 30$ K. The data can be better described by the combination of TA and TE effects (TA + TE). Inset shows the histogram of the estimated relative TE coefficient of AuNP to that of the substrate, $\Delta\alpha$. As marked by the vertical line, the predicted $\Delta\alpha$ for Si substrate using bulk coefficients is roughly 1.3×10^{-5} K^{-1}.

our deposition scheme were not always closely packed and regular, R_T for a specific molecule modification varied from sample to sample. To clarify the role of RT resistance in the MIT, we reduced the junction barrier height of insulating MOA devices by applying high-dosage e-beam exposure. The e-beam exposure greatly reduced the RT resistance and transformed some devices (typically $R_{RT} < R_K$) to metallic. Compared to the spacing control method using molecule engineering, this e-beam exposure method provides us with more precise control of R_T. By assuming that $R_{RT} \approx R_T$ in most of our devices, we could find that a clear separation of metallic and insulating properties was narrowed down to $10^4 < R_T < 10^5$ Ω, a value comparable to R_K. This result suggests that the RT resistance, rather than s, is more important for judging the metallic and insulating behaviours of a device.

3.2 Thermal activation behaviour and the effect of thermal expansion

A widely accepted R *vs.* T behaviour for weakly coupled NP assemblies follows the expression $R(T) \propto \exp(T_1/T)$, which describes a thermal activation (TA) property in which the charges encounter a characteristic energy barrier of $E_a = k_B T_1$ in a system overwhelmed by nearest-neighbour hopping, as is schematically shown in Fig. 1b. However, a careful inspection reveals a slight deviation, which can be explained by the different thermal expansion (TE) of the AuNPs and the substrate.[24,25] The anomalous peak at 235 K in the $R(T)$ curves gives another piece of evidence that $R(T)$ is affected by substrate expansion and contraction (Sec. IV, ESI†). It is believed that this peak structure demonstrates the homogeneous nucleation of super-cooled water trapped inside the nanoporous AuNP network during the film formation.[24]

To combine the TA and TE effects, we assumed the following fitting formula:

$$R(T) = R_1 \exp(\gamma T)\exp(T_1/T), \quad (1)$$

in which the fitting parameter γ can be expressed by $\gamma = -\beta(2r+s)\Delta\alpha$ to experimentally give the difference of linear TE coefficients of Au and the substrate, $\Delta\alpha = \alpha_{Au} - \alpha_{sub}$. In Fig. 1c we compare the fitting results for a MUA device using the TA model only and using combined TA and TE models. Ideally the Si substrate would result in a positive $\Delta\alpha \approx 1.3 \times 10^{-5}$ K^{-1}, whereas the polyimide (PI) substrate would yield a negative $\Delta\alpha \approx -4.1 \times 10^{-5}$ K^{-1}. The experimental results illustrated in the inset of Fig. 1c confirm the opposite trends for the two substrates but underestimated the $\Delta\alpha$ value for PI.

3.3 Activation energy and the critical point

The quantum fluctuation model asserts that the finite lifetime of charge in a NP gives the reduced activation energy $E_a \approx E_C(1 - 4\pi^{-1}zg \ln 2)$, in which z is the number of nearest neighbour NPs.[1] The Abeles formula $E_C = (8\pi\kappa_m\varepsilon_0)^{-1}e^2sr(s+r)^{-1}$ gives a precise estimation of the charging energy for a single NP embedded in assemblies or networks.[28] The parameter $\kappa_m \approx 2.6$ is the dielectric constant of the linkage molecule. The theoretical values are roughly 2 times greater than the experimental results as reported in most previous works. This over-estimation in charging energy is likely due to the random charge offsets distributed all over the NP assembly.[29] With these charge offsets, the energy cost for single charge tunnelling through a molecular junction will range between 0 and E_C, giving an average value of $E_C/2$. For a regular NP network, one can estimate R_T from the (monolayer) sheet resistance R_s at a temperature $T \gg E_a/k_B = T_1$. For most devices we studied, RT is high enough for us to estimate $R_T \approx R_s$; therefore, we can plot T_1 as a function of (RT) R_s in Fig. 2. Since E_C relates to R_T by using $s \propto \beta^{-1} \ln R_T \approx \beta^{-1} \ln R_s$, we can plot calculated $E_C/2$ and $E_a/2$ in

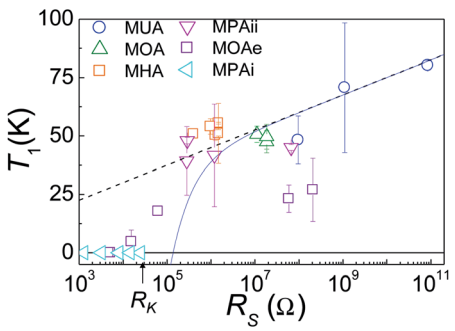

Fig. 2 The activation energy T_1 as a function of sheet resistance at RT. The error bar describes the uncertainty in T_1 by using two fitting models (TA and TA + TE). The solid curve and dashed curve represent the theoretical calculated $E_a/2$ and $E_C/2$. The critical point is close to the prediction of the quantum fluctuation model.

the figure as well. The data agree well with the $E_a/2$ prediction, which includes both the random charge offset and charge fluctuation, indicating a critical point of the Mott–Hubbard MIT at $R_T = R_K$. Although most insulating devices can be described well with the quantum fluctuation model, we would like to note that MPAi devices follow a different type of insulating property: despite having a low R_s and a zero Hubbard gap, their resistance increases rapidly when $T < 1$ K. There are indications that their behaviours are closely related to disorder, outside the scope of Mott–Hubbard theory.

3.4 Co-tunnelling in molecular junctions

When the temperature is lower than 20 K, insulating samples exhibit a $\ln R \propto T^{-1/2}$ dependence (see Fig. 3a), which can be explained by the Efros–Shklovskii (E–S) variable range hopping (VRH) model.[30,31] The E–S VRH describes a system in which Coulomb interaction between electrons is significant, which is also confirmed in the non-linear current–voltage (IV) curve at low temperatures, signifying the effect of the Coulomb gap. As highlighted in recent theoretical works, the co-tunnelling for a large junction array would yield an E–S VRH property, describing the effect of balancing the charge hopping distance and energy cost.[20,21] From the above findings, we picture that the charge conduction in the AuNP films is from high-temperature nearest-neighbour hopping to low-temperature variable range co-tunnelling (or VRH).

The co-tunnelling, which describes the collective motion of electrons in nearby AuNPs as shown in Fig 3d, would effectively transfer the electron with a long distance, similar to long-range hopping. It consists of elastic and inelastic channels, which would be separated by a crossover temperature, $T_{cross} \approx 0.1\sqrt{E_C\delta}$, above which the inelastic channel dominates.

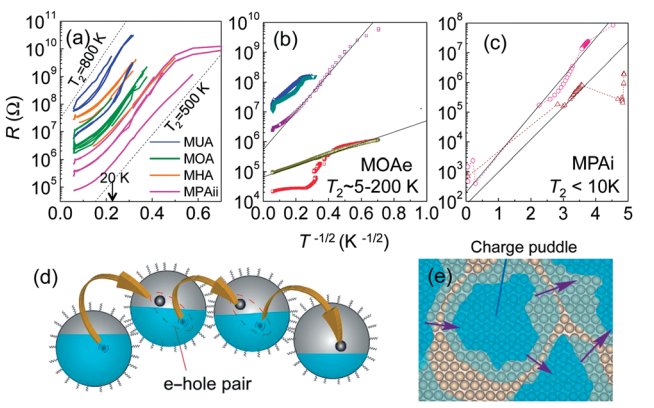

Fig. 3 R vs. $1/T^{1/2}$ plots for insulating devices (a): at $T < 20$ K, Mott insulating devices transform to E–S VRH behaviour, with the characteristic temperature ranging from 500 to 800 K. (b) Insulating MOAe devices show T_2 ranging from 5 to 200 K, relating to their R_{RT} values. (c) The MPAi devices have a typical $T_2 < 10$ K, in the temperature range $T < 1$ K. (d) The schematic of inelastic co-tunnelling in Mott insulators, in which charges are localized in a single NP. (e) By contrast, the co-tunnelling in Anderson insulators occurs in-between charge puddles forming in clusters of NPs.

The electron level spacing, δ, of the 12 nm AuNP is roughly 0.1 meV so $T_{cross} \approx 2$ K in our system, suggesting that most insulating devices should be discussed within the scope of the inelastic channel. The inelastic co-tunneling yields an exponentially suppressed hopping probability, $\propto \exp(-r_{ij}/l_{in})$ on the distance r_{ij} of NP i and j. However, unlike the standard E–S model, the localization length $l_{in} \approx 2a/\ln(E^2/16\pi k_B{}^2T^2g)$ is temperature-dependent. Here, a is the average NP center-to-center distance, and E is the average energy for electron and hole excitation energies, roughly on the order of E_a. There exists an optimal range of charge hopping because of competition between the above hopping probability and the Arrhenius factor $\propto \exp(-U/k_BT)$ owing to long-range Coulomb repulsion, $U = e^2/\kappa\varepsilon_0 r_{ij}$.[1] Here, κ is the effective dielectric constant of the NP assembly so one should not confuse it with κ_m. By maximizing the overall hopping probability, one gets the optimal hopping distance $r^* \approx (l_{in}e^2/k_BT\kappa\varepsilon_0)^{1/2}$, and the optimal hopping probability $\approx \exp(-2r^*/l_{in})$. Because l_{in} only slowly varies with T, the optimal charge hopping probability would follow an $\exp(T^{-1/2})$ dependence. For MOA and MHA insulating devices, in which $g \approx 0.01$, the factor $\ln(E^2/16\pi k_B{}^2T^2g) \approx 2.5$ at $T = 20$ K, whereas it is ~7.1 at $T = 2$ K. In such a picture we require $l_{in} \leq a$ for a weak coupling case (namely $g < 1$). The above derivation asserts a characteristic temperature $k_BT_2 \approx 2.8e^2/\kappa\varepsilon_0 l_{in}$, which allows us a comparison with the experiment.[1] On the other hand, the experimental T_2 value ranges from 500 to 1300 K, giving an effective κ of 90–270, much larger than κ_m by using $l_{in} \approx a$. Such a discrepancy can be understood by the charge-screening effect from localized background electrons, which gives the dielectric constant an enhancement of $\kappa_{Au} \approx 1+4\pi e^2N(E_F)l_{in}/\varepsilon_0$, where $N(E_F)$ is the Au density of state at the Fermi energy E_F. Again, $l_{in} \approx a$, an estimation gives $\kappa_{Au} \approx 24e^2/\varepsilon_0 a\delta \approx 520$, close to the experimental value. We also note that due to a large particle size, we have a larger effective dielectric constant than that reported on a 5 nm NP assembly; a previous work on a similar VRH phenomenon considered κ to be around 4, $\sim\kappa_m$.[20]

MOAe devices showed a much smaller T_2 than other Mott insulators. Other works which reported small T_2 values either argued a small pre-factor[32] or assumed the scenario of quasi-localized hopping.[14] Although such a problem is still under debate as pointed out in a recent review,[2] we believe that disorder plays an important role in the MOAe cases. Imagining that the structure disorder and electrostatic (charge offset) disorder would create longer tails at the band edge, it turns the hard Hubbard gap to a soft Coulomb gap when the system is driven closer to the transition. Indeed, one can find that MOAe devices, which can be categorized as disordered Mott insulators, systematically have smaller T_1 values than other insulators. Of course, the smaller gap allows a larger localization length and a greater dielectric constant due to charge screening.

The inelastic co-tunnelling would feature IV characteristics following a power law, $I \propto V^{2j-1}$, in the voltage region $k_BT < eV < -k_BT\ln(g)$. The parameter $j \approx (-E_C/k_BT\ln(g))^{1/2}$ is the number of junctions involved in a multiple co-tunnelling.[22] In Fig. 4 we present log–log plot of the IV curves at low temperatures, where the exponents $2j-1$ are found to be 2–3, 1.6 and ~1 for MUA (at $T = 20$ K), MOA ($T = 9$ K) and MHA ($T = 7$ K) devices. The

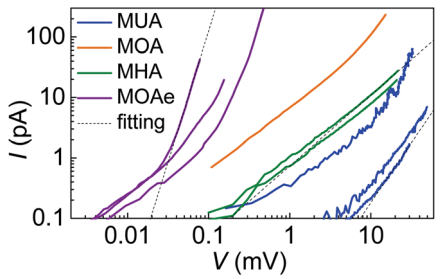

Fig. 4 The *IV* characteristics of Mott insulators show a power law behaviour in the high-field regime. The exponent indicates how much junctions are involved in a multiple co-tunnelling.

e-beam exposed MOAe devices at $T = 2$ K would give a larger $2j - 1$, around 4 in this power-law regime.

3.5 Anderson insulators

As has been mentioned before, the disorder, which is due to structure irregularity and/or electrostatic inhomogeneity, is crucial for systems near the MIT such as MPAi devices. Having a zero Hubbard gap, their insulating property can only be identified when cooled below 1 K: they exhibit non-linear *IV* curves and $R(T)$ curves of $\ln R \propto T^{-1/2}$ as shown in Fig. 3c. Although this temperature dependence is similar to that of disordered Mott insulators, the different mechanism concludes that MPAi devices fall into a different category of insulator, the Anderson insulators.[19] In disordered Mott insulators, the E–S VRH behaviour is due to the co-tunnelling of molecular junctions, whereas in Anderson insulators, the localization length expands to form charge puddles, the sizes of which are much greater than the NP size. Indeed, ref. 17 reported that these devices could demonstrate very interesting single charge tunnelling and resonate tunnelling at mK temperatures, from which a charge puddle size as large as 100 nm was confirmed. The T_2 values for these samples are similar, suggesting a likelihood of disorder strength and localization length, despite a large variation in the tunnelling resistance.

The magnetoresistance (MR) unveils how the quantum interference affects the charge inhomogeneity in the Anderson insulators. For Mott insulators we could not observe clear magnetic-field modulations except for two special cases. By contrast, devices that are categorized as Anderson insulators all exhibit relatively pronounced magnetic-field modulation: their Coulomb gap shrinks in a high magnetic field parallel or perpendicular to the NP film, presenting a magnetic field-induced de-localization of electrons (see Fig. 5a). The magnetic field produces additional Aharonov–Bohm phases to destroy the constructive interference of electron back-scattering, namely Anderson localization. Indeed, such a breakdown of quantum interference can be confirmed by the magnetoresistance of the metallic AuNP assemblies shown in Fig. 5b. We can observe pronounced weak anti-localization,[33] which is due to strong spin–orbital interaction of Au below the temperature of 2 K.

Would the concept of Anderson insulator be simulating the weak localization in disordered metals? Apparently not. First,

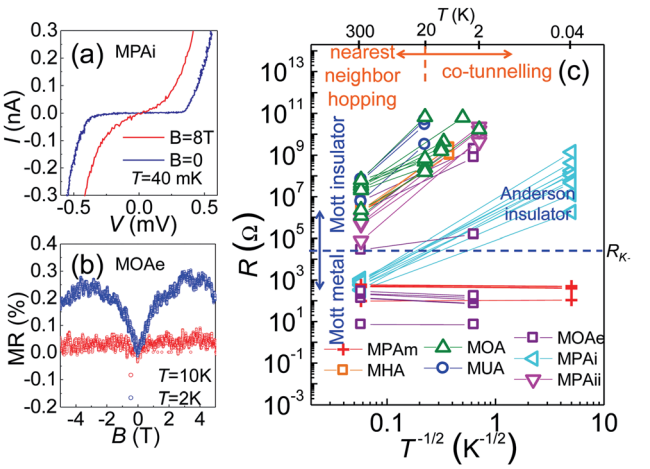

Fig. 5 (a) MPAi Anderson insulators can exhibit magnetic field-modulated *IV* characteristics at a sufficiently low temperature. (b) Metallic MOAe devices present weak anti-localization at a temperature $T < 2$ K. The field is perpendicular to the substrate. (c) *R vs.* $T^{-1/2}$ curves for all devices. The data illustrated here were measured at RT and $T =$ 40 mK, 40 mK, 2 K, and 2.5 K respectively for MPAm, MPAi, MPAii and MOAe devices.

the resistance increment of the MPAi devices below $T = 1$ K can be as large as 3 orders of magnitude, whilst typical weak localization only results in a resistance change of a few percent. Second, the MR found in the Anderson insulators is negative, opposite to that in Au metals, in which the strong spin–orbital interaction should result in weak anti-localization. Third, the weak localization only produces the universal conductance fluctuation as the gate modulation in samples whose size is smaller than the dephasing length.[34,35] However, the single electron tunneling and/or resonance tunnelling observed in MPAi devices indicates strong localization of charge and the formation of charge puddles.

We summarize the charge conduction property of AuNP films in the *R*–*T* parameter space as shown in Fig. 5c. When $R_s > R_K$, the sample is a Mott insulator, which gives a thermal activation *R* due to a hard gap, E_a, in the density of state. For Mott insulators, the dominant charge conduction evolves from nearest neighbour hopping to co-tunnelling, which is contributed from some localized electronic states due to finite disorder. When $R_s \approx R_K$, a sample with finite disorder may be an Anderson insulator, which features a co-tunnelling between charge puddles. In this case the temperature-dependent soft gap is formed at the Fermi level.

3.6 Interparticle spacing controlled by strain

In the last part we discuss the charge conduction in AuNP films when the substrate is elongated or compressed by bending. One should bear in mind that the interparticle spacing change, Δs, as well as the film resistivity are not isotropic: the resistance change is maximal when the current is parallel to the bending direction so we focus on this parallel measurement configuration. As illustrated in Fig. 6a, the resistance as a function of the spacing change due to the strained substrate follows an

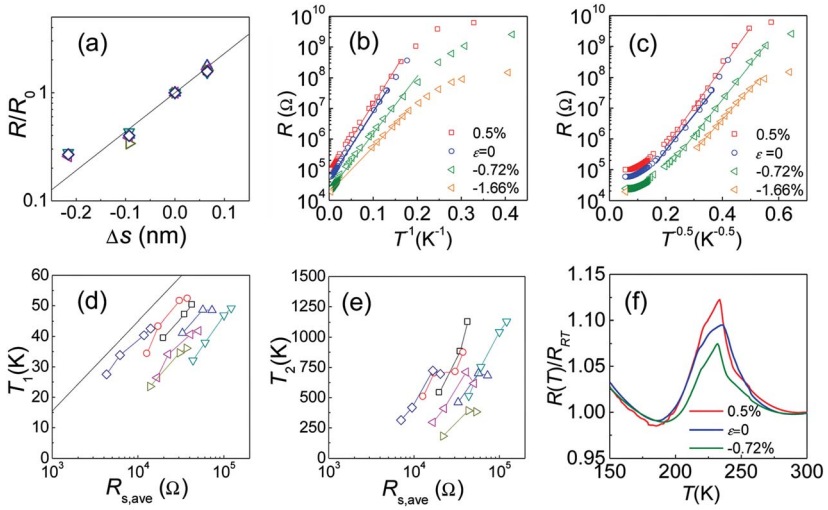

Fig. 6 (a) Devices under strain present a RT resistance following an exponential dependence on the estimated Δs. Because of the anisotropic change in s, the resistance roughly follows $R/R_0 = \exp(\beta_a \Delta s)$, in which β_a is about 8 nm^{-1} smaller than the isotropic change in s. (b) The R *vs.* $1/T$ plots for one MPAp device under different strain. The thermal activation energy reduces when a compressive strain is applied to the substrate. (c) At $T < 20$ K, the resistance also follows E–S VRH behaviour. Again, the characteristic temperature T_2 becomes smaller when the substrate is compressed. (d) T_1 as a function of average sheet resistance $R_{s,ave}$ for several MPAp devices. We found an exponential relation, $T_1 \approx \ln R_{s,ave}$, without showing a clear quantum fluctuation effect in these devices. The solid line shows the calculated E_C as a function of $R_{s,ave}$. (e) T_2 as a function of $R_{s,ave}$. (f) The anomalous resistance peak at 225 K has a smaller height when the substrate is compressed. The additional compression squeezes out trapped water molecules in the NP network so as to reduce the effect of water freezing.

exponential law. Furthermore the temperature dependence of the resistance follows the thermal activation behaviour when $T > 20$ K, but obeys the E–S VRH when $T < 20$ K as respectively shown in Fig. 6b and 6c. One can clearly see that the characteristic temperatures T_1 and T_2 increase as the strain increases. To systematically analyze the change of T_1 and T_2, we first evaluate the average resistance of the film with strain as $R_{s,ave} = 2/({R_{s0}}^{-1} + {R_s}^{-1})$. Here, R_{s0} is the sheet resistance without strain, whereas R_s is the parallel sheet resistance with strain. They provide the estimation of tunnelling resistances in the two principal directions. Presumably the effect of quantum fluctuation depends on the average sheet resistance,[36] so we plot T_1 as a function of $R_{s,ave}$ (see Fig. 6d). Again we find that T_1 increases as $R_{s,ave}$ increases, following an exponential behaviour as shown in Fig. 2.

4 Conclusions

In summary, we studied the overall charge conduction in thin films made of self-assembled gold nanoparticles. We used several schemes to tune the interparticle tunnelling resistance: by controlling the interparticle spacing and the tunnelling barrier height. The temperature-dependent film resistances reveal that the films undergo a Mott–Hubbard MIT as the monolayer sheet resistance approaches to the quantum resistance. The high-temperature $R(T)$ curves show a thermal activation behaviour, featuring nearest-neighbour hopping with a quantum fluctuation re-normalized charging energy. At low temperatures, the charge conduction turns into the inelastic co-tunnelling with a characteristic temperature of about 700 K, reflecting an effective dielectric constant of about 200. By applying strain to the substrate, we can control the interparticle spacing of a specific device and determined how the activation energy and VRH temperature change as a function of the tunnelling resistance. We also discovered Anderson insulators when the tunnelling resistance is lower than the threshold of a Mott insulator but with a robust disorder. They only present tunnelling between charge puddles due to inhomogeneity, which can be smeared out in a large magnetic field.

Acknowledgements

The authors acknowledge J. C. Chen, W. B. Jian and J. J Lin for fruitful discussions. This work was supported by the National Science Council of Taiwan through Grant no. NSC102-2628-M-005-001-MY4 and NSC102-2112-M-259-002-MY3.

Notes and references

1 I. Beloborodov, A. Lopatin, V. Vinokur and K. Efetov, *Rev. Mod. Phys.*, 2007, **79**, 469.
2 A. Zabet-Khosousi and A. A. Dhirani, *Chem. Rev.*, 2008, **108**, 4072–4124.
3 A. W. Snow and H. Wohltjen, *Chem. Mater.*, 1998, **10**, 947–949.
4 C. P. Collier, R. J. Saykally, J. J. Shiang, S. E. Henrichs and J. R. Heath, *Science*, 1997, **277**, 1978–1981.
5 J. M. Wessels, H.-G. Nothofer, W. E. Ford, F. von Wrochem, F. Scholz, T. Vossmeyer, A. Schroedter, H. Weller and A. Yasuda, *J. Am. Chem. Soc.*, 2004, **126**, 3349–3356.
6 R. Parthasarathy, X.-M. Lin and H. M. Jaeger, *Phys. Rev. Lett.*, 2001, **87**, 186807.

7 P. E. Trudeau, A. Orozco, E. Kwan and A. A. Dhirani, *J. Chem. Phys.*, 2002, **117**, 3978.
8 A. A. Middleton and N. S. Wingreen, *Phys. Rev. Lett.*, 1993, **71**, 3198–3201.
9 K. H. Müller, G. Wei, B. Raguse and J. Myers, *Phys. Rev. B: Condens. Matter Mater. Phys.*, 2003, **68**, 155407.
10 Y.-L. Lo, S.-J. Sun and Y.-J. Kao, *Phys. Rev. B: Condens. Matter Mater. Phys.*, 2011, **84**, 075106.
11 D. Conklin, S. Nanayakkara, T.-H. Park, M. F. Lagadec, J. T. Stecher, M. J. Therien and D. A. Bonnell, *Nano Lett.*, 2012, **12**, 2414–2419.
12 I. S. Beloborodov, K. B. Efetov, A. V. Lopatin and V. M. Vinokur, *Phys. Rev. Lett.*, 2003, **91**, 246801.
13 R. H. Terrill, T. A. Postlethwaite, C.-h. Chen, C.-D. Poon, A. Terzis, A. Chen, J. E. Hutchison, M. R. Clark and G. Wignall, *J. Am. Chem. Soc.*, 1995, **117**, 12537–12548.
14 J. L. Dunford, Y. Suganuma, A. A. Dhirani and B. Statt, *Phys. Rev. B: Condens. Matter Mater. Phys.*, 2005, **72**, 075441.
15 N. F. Mott, *Rev. Mod. Phys.*, 1968, **40**, 677.
16 A. Zabet-Khosousi, P. Trudeau, Y. Suganuma, A. Dhirani and B. Statt, *Phys. Rev. Lett.*, 2006, **96**, 156403.
17 C.-W. Jiang, I. C. Ni, S.-D. Tzeng and W. Kuo, *Appl. Phys. Lett.*, 2012, **101**, 083105–083104.
18 A. J. Houtepen, D. Kockmann and D. Vanmaekelbergh, *Nano Lett.*, 2008, **8**, 3516–3520.
19 K. Byczuk, W. Hofstetter and D. Vollhardt, *Phys. Rev. Lett.*, 2005, **94**, 56404.
20 T. Tran, I. Beloborodov, X. Lin, T. Bigioni, V. Vinokur and H. Jaeger, *Phys. Rev. Lett.*, 2005, **95**, 76806.
21 T. B. Tran, I. S. Beloborodov, J. Hu, X. M. Lin, T. F. Rosenbaum and H. M. Jaeger, *Phys. Rev. B: Condens. Matter Mater. Phys.*, 2008, **78**, 075437.
22 J.-F. Dayen, E. Devid, M. V. Kamalakar, D. Golubev, C. Guédon, V. Faramarzi, B. Doudin and S. J. van der Molen, *Adv. Mater.*, 2013, **25**, 400–404.
23 P. W. Anderson, *Phys. Rev.*, 1958, **109**, 1492.
24 K. H. Müller, J. Herrmann, G. Wei, B. Raguse and L. Wieczorek, *J. Phys. Chem. C*, 2009, **113**, 18027–18031.
25 M. M. A. Yajadda, K. H. Müller and K. Ostrikov, *Phys. Rev. B: Condens. Matter Mater. Phys.*, 2011, **84**, 235431.
26 I. C. Ni, S. C. Yang, C. W. Jiang, C. S. Luo, W. Kuo, K. J. Lin and S. D. Tzeng, *J. Phys. Chem. C*, 2012, **116**, 8095–8101.
27 B. Xu and N. J. Tao, *Science*, 2003, **301**, 1221–1223.
28 B. Abeles, *Phys. Rev. B: Solid State*, 1977, **15**, 2828–2829.
29 T. Sugawara, M. Minamoto, M. M. Matsushita, P. Nickels and S. Komiyama, *Phys. Rev. B: Condens. Matter Mater. Phys.*, 2008, **77**, 235316.
30 A. L. Efros and B. I. Shklovskii, *J. Phys. C: Solid State Phys.*, 1975, **8**, L49.
31 A. Efros and B. Shklovskii, *Springer Series in Solid-State Sciences*, Springer, Berlin, 1984.
32 Y. Noguchi, T. Terui, T. Katayama, M. M. Matsushita and T. Sugawara, *Appl. Phys. Lett.*, 2011, **98**, 263114–263113.
33 G. Bergmann, *Phys. Rep.*, 1984, **107**, 1–58.
34 S. B. Kaplan and A. Hartstein, *Phys. Rev. Lett.*, 1986, **56**, 2403–2406.
35 P. A. Lee, A. D. Stone and H. Fukuyama, *Phys. Rev. B: Condens. Matter Mater. Phys.*, 1987, **35**, 1039–1070.
36 See ESI† for the derivation.